Quantitative elemental analysis of a specimen in air via external beam laser-driven particle-induced x-ray emission with a compact proton source

Martina Salvadori,[1,*] Fernando Brandi,[1,†] Luca Labate,[1,‡,§] Federica Baffigi,[1] Lorenzo Fulgentini,[1] Pietro Galizia,[2] Petra Koester,[1] Daniele Palla,[1] Diletta Sciti,[2] and Leonida A. Gizzi[1,§]

[1] *Consiglio Nazionale delle Ricerche, Istituto Nazionale di Ottica (CNR-INO), Pisa, Via Moruzzi, 1, Pisa 56124, Italy*

[2] *Consiglio Nazionale delle Ricerche, Istituto di Scienza, Tecnologia e Sostenibilità per lo Sviluppo dei Materiali Ceramici (CNR-ISSMC), Faenza, Italy*

(Received 15 December 2023; revised 22 March 2024; accepted 10 May 2024; published 10 June 2024)

Particle-induced x-ray emission (PIXE) is a well-established ion-beam analysis technique, enabling quantitative measurement of the elemental composition of a sample surface under an ambient atmosphere with an *external beam*, which significantly simplifies the measurements, and is strictly necessary for those samples that cannot sustain a vacuum environment. Few-MeV electrostatic proton accelerators are used today in PIXE systems. We present here an external beam PIXE methodology based on a compact laser-driven proton accelerator. A 10-TW class ultrashort laser is used to generate a few-MeV proton beam, and a compact transport magnetic beamline is used to collect and transport the proton beam and to prevent unwanted fast electrons from reaching the sample. An x-ray CCD camera in single-photon detection mode is used to retrieve the spectrum of radiation emitted by the samples upon proton irradiation in air. Elemental composition analysis is performed and validated against standard energy-dispersive x-ray spectroscopy, demonstrating quantitative and accurate external beam PIXE analysis with compact laser-driven accelerators.

DOI: 10.1103/PhysRevApplied.21.064020

I. INTRODUCTION

The ultraintense pulsed laser-matter interaction for proton acceleration has been studied for more than two decades [1,2] and is nowadays routinely implemented in many research laboratories worldwide. Appealing features of laser-driven particle accelerators include their very compact footprint and the intrinsically short bunch duration. Historically, proton beams with energies up to several tens of MeV were reported using large-scale high-energy ($\sim$ 100 J) laser systems, the repetition rate of which was usually limited to a fraction of a Hz. Acceleration of protons is achieved through the so-called target normal sheath acceleration (TNSA) process [3–5]; in this process, populations of fast electrons (up to the MeV range) are accelerated at the front side of a thin solid target and then propagate through the overdense target, exiting the back surface, to induce a strong electric field (up to TV/m), thereby accelerating protons and light ions at the rear side of the target. Although being underpinned by a wealth of different laser-target and fast-electron-transport processes, the full understanding of which is still an ongoing process and requires advanced theoretical and numerical tools, TNSA is nowadays routinely exploited in several laboratories worldwide to accelerate protons and light ions. Over the past decade or so, ultrashort and ultraintense laser pulses with moderate energy (1–10 J) have also been used for this purpose [6–8], with the added value of allowing, in principle, high-repetition-rate (i.e., high average flux) beams to be produced. Moreover, advanced nanostructured solid targets [9–13] have also been proposed to enhance efficiency and increase the intensity of the proton pulse. Furthermore, proton-acceleration regimes based on phenomena such as relativistic induced transparency and/or radiation pressure acceleration [14–16] have been found to enable the acceleration of beams with $\gtrsim$100-MeV energy. This kind of study has been carried out using 100-TW class laser systems.

On the other hand, few-MeV proton beams can be efficiently accelerated, via TNSA, with smaller-scale 10-TW class lasers. Such sources can, in principle, provide an

*Corresponding author: martina.salvadori@ino.cnr.it
†Corresponding author: fernando.brandi@ino.cnr.it
‡Corresponding author: luca.labate@ino.cnr.it
§Also at Istituto Nazionale di Fisica Nucleare (INFN), Sezione di Pisa, Italy.

alternative to the usage of conventional proton accelerators (TANDEM, cyclotrons, etc.), with appealing features such as the flexibility of a fully optical setup and the reduced requirements for ionizing-radiation shielding, made possible by the acceleration processes taking place over very small distances. Also, modern compact 10-TW class laser systems can fit on a standard optical table and the complete laser-driven accelerator can be placed in a standard laboratory room. In general, given the maturity and potential of laser-driven particle acceleration, much effort is currently devoted to search for actual implementations of laser-driven compact accelerators, of either electrons or protons (light ions), in real practical applications beyond basic research and proof-of-principle experiments. Notable examples span from large international projects, aiming at high-quality electron-accelerator facilities [17], to the very rapidly growing interest in accelerators for radiotherapy based on laser-driven sources [18–20].

Different types of energetic particles and electromagnetic radiation are produced during ultrahigh-intensity laser-matter interactions, like electrons, protons, light ions, and characteristic x-ray radiation, which can also be used to generate secondary radiation, like neutrons, positrons, and bremsstrahlung. These kinds of energetic particles and radiation can be applied to perform material characterization analysis, for example, x-ray fluorescence (XRF) [21], activation analysis [22], radiography [23], and positronium annihilation lifetime spectroscopy [24]. In this context, few-MeV proton beams are well suited for nondestructive analysis via particle-induced x-ray emission (PIXE), which is a well-established technique used to characterize quantitatively the elemental composition of a sample surface through the spectral analysis of the characteristic x-ray radiation emission induced by particle irradiation [25–27]. A very relevant specificity of the PIXE technique is the possibility to perform sample irradiation under an ambient atmosphere by letting the proton beam propagate in air, i.e., *external beam* PIXE. This approach has several advantages and greatly simplifies the implementation of PIXE, by speeding up the analysis of a large amount of samples [28,29], and by reducing sample charging and heating, therefore minimizing possible damage to delicate specimens. Notably, external beam PIXE is *strictly necessary* in those cases where samples cannot sustain a vacuum environment or be placed inside a vacuum chamber, like specimens with volatile components, delicate cultural heritage objects, and biological samples [30,31]. Today, PIXE systems are based on bulky and massive electrostatic proton accelerators; there is however growing interest in developing smaller-scale PIXE systems, for example, based on a 2-MeV rf-driven compact accelerator [32]. The use of laser-driven few-MeV proton accelerators for PIXE is extremely appealing, and it has been recently investigated theoretically through simulations [33–37], as well as with experiments employing relatively large high-power laser systems with the sample in a vacuum [38–40].

Here, we introduce the external beam laser- (EBL) driven PIXE technique and report on the development, characterization, and validation of a practical system based on a relatively simple design comprising (i) a compact few-MeV TNSA-based proton source; (ii) an efficient magnetic quadrupole beam line used to transport the protons from the source to air; and (iii) a CCD camera in single-photon detection mode used for the spectral analysis of the x-ray emitted by the sample under investigation. The performances of EBL PIXE are assessed, first in terms of the characteristics and stability of the laser-driven proton beam, and then with actual PIXE measurements on a multi-element sample validated through quantitative comparison with standard energy-dispersive x-ray spectroscopy (EDS) analysis.

II. RESULTS AND DISCUSSION

A schematic representation of the compact EBL-PIXE system is given in Fig. 1, and a picture of the irradiation site in air is shown as the inset. The Ti:sapphire 14-TW 10-Hz beamline at the Intense Laser Irradiation Laboratory of the CNR-INO in Pisa [41] is used to drive the TNSA-based proton source. The laser-beam intensity on the target was approximately 4×10^{19} W cm^{-2}, see the Supplemental Material for technical details [42]. A 5-μm-thick titanium foil was used as a target, to accelerate proton beams via the TNSA process. In the present measurements, the target position was refreshed after each laser shot with a maximum frequency of about 0.1 Hz, limited by the target movement and alignment system; repetition rates up to 10 Hz are feasible with a rapidly moving foil, for example, a rolling-tape target [43,44]. The laser-driven proton beam propagates in the direction normal to the rear surface of the target with a divergence of about 15° HWHM, typical of few-MeV TNSA proton beams [45,46]. To efficiently transport the protons from the source to the application site, a MBL can be used [47,48]. For EBL PIXE, we designed a modular and cost-effective MBL composed of a sequence of magnetic quadrupoles based on commercial neodymium permanent magnets of $25 \times 12 \times 4$ mm^3 in dimension, embedded in soft iron supporting cages. The first two quadrupoles facing the TNSA target are designed with a 25×25 mm^2 clear aperture, while the others have 12×12 mm^2 clear apertures. The MBL is placed at 12.5 mm from the proton source, which is 24.9 cm long, and the quadrupoles' orientations alternate along the line, as shown in Fig. 2(a). To enable proton-beam optimization and characterization with and without magnetic transport, the MBL was moved in and out of the beam path via a motorized stage. The transported proton beam was finally allowed to propagate under an ambient atmosphere through a 13-μm-thick circular Kapton window.

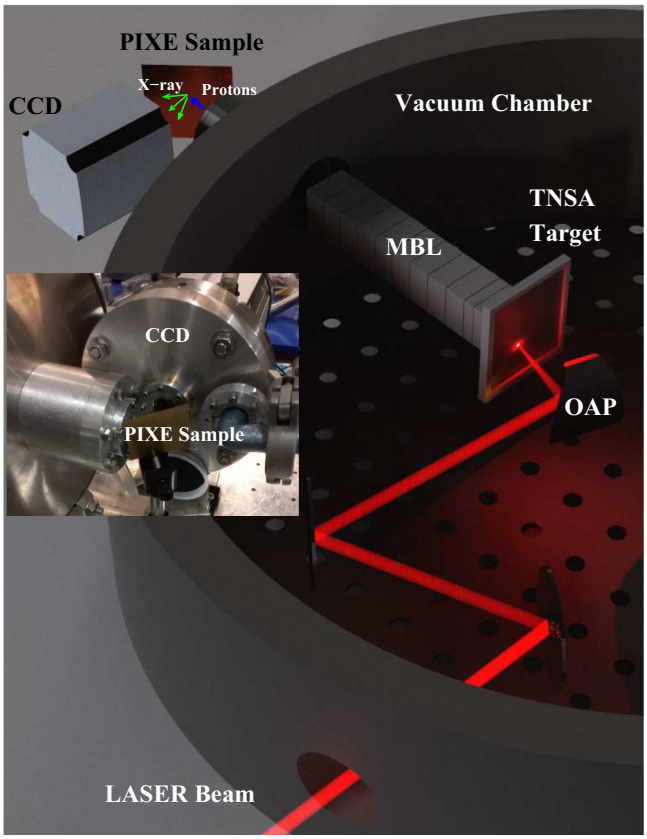

FIG. 1. Representation of the EBL-PIXE system showing the main components (not to scale): TW laser beam, off-axis parabolic mirror (OAP), magnetic beamline (MBL), PIXE sample, and x-ray CCD; proton beam and x-ray are represented by blue and green arrows, respectively; TNSA proton source and MBL are contained in a vacuum chamber, PIXE sample is in air, and CCD chip is kept in a separate vacuum environment; inset shows a picture of the actual EBL-PIXE irradiation site.

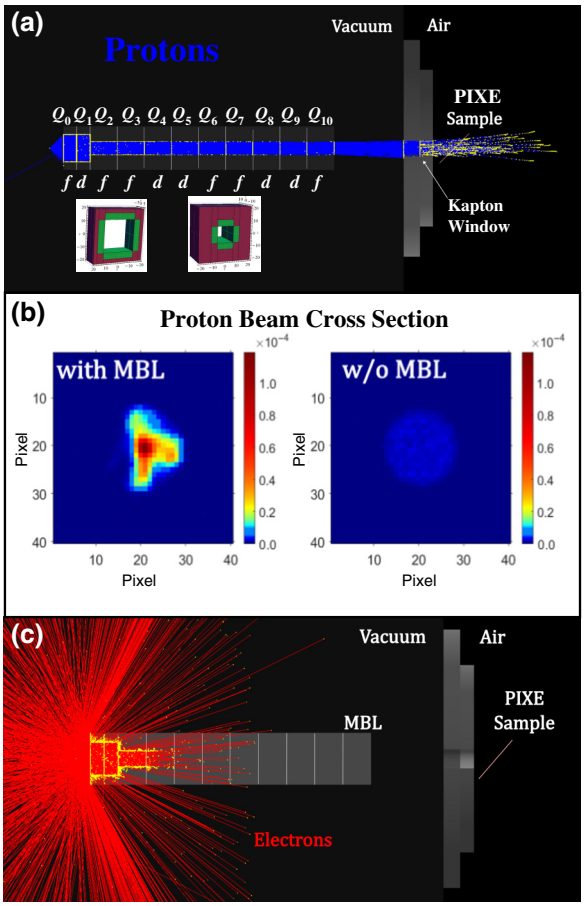

FIG. 2. MBL design and characteristics. (a) MBL schematic with the PIXE sample location indicated and the simulated proton-beam transport; "f" and "d" indicate the alternating orientation of the magnetic field in the 11 quadrupoles denoted by Q_i, $i = 0$–10; schematic of the two quadrupole magnet types are shown in the two insets. (b) Cross-section distribution of the simulated proton beam at the PIXE sample location in air with and without (w/o) MBL, left and right panels, respectively, where a pixel area corresponds to 1 mm^2; circular shape of the simulated beam is due to the Kapton window used as the vacuum-air interface. (c) Simulation of propagation in the MBL of fast electrons from the laser-driven source.

The PIXE sample was placed under an ambient atmosphere at 2 cm from the Kapton window with the surface oriented at 45° with respect to the MBL axis. The spectrum of the x-ray emitted by the sample upon proton irradiation was measured shot by shot with a CCD camera (ANDOR, IKON-M) acquired in the single-photon regime [49] and placed at 90° with respect to the MBL axis, as shown in Fig. 1. The analysis to retrieve the energy spectrum from the raw CCD data was carried out using the procedure described in Ref. [50]. Further details on the CCD setup can be found in the Supplemental Material [42]; here we only mention that the low-energy cutoff of our spectral measurements was about 5 keV.

The MBL performance was studied with Monte Carlo simulations based on the Geant4 toolkit [51], as described in Ref. [52]. The transverse view of the simulated proton beam is reported in Fig. 2(a). The proton source used in the simulations is described by a TNSA-like exponentially decreasing energy spectrum with a sharp cutoff at 3 MeV and temperature of 0.8 MeV, as from data obtained experimentally. The resulting cross-section profile of the proton beam in air is reported in the left panel of Fig. 2(b). For comparison, the cross-section profile of the proton beam in air simulated without the MBL is shown in the right panel of Fig. 2(b). The calculated enhancement factor of the integrated flux per shot with the MBL compared with the case without the MBL is about 8.5. Notably, the MBL also has the fundamental effect of removing the TNSA fast electrons from the proton-beam path, which is absolutely necessary for quantitative PIXE analysis, since the interaction of such fast electrons with the sample also efficiently generates x-ray emission; this would result in a significant spurious contribution to the total x-ray signal. In Fig. 2(c), a Geant4 simulation showing the

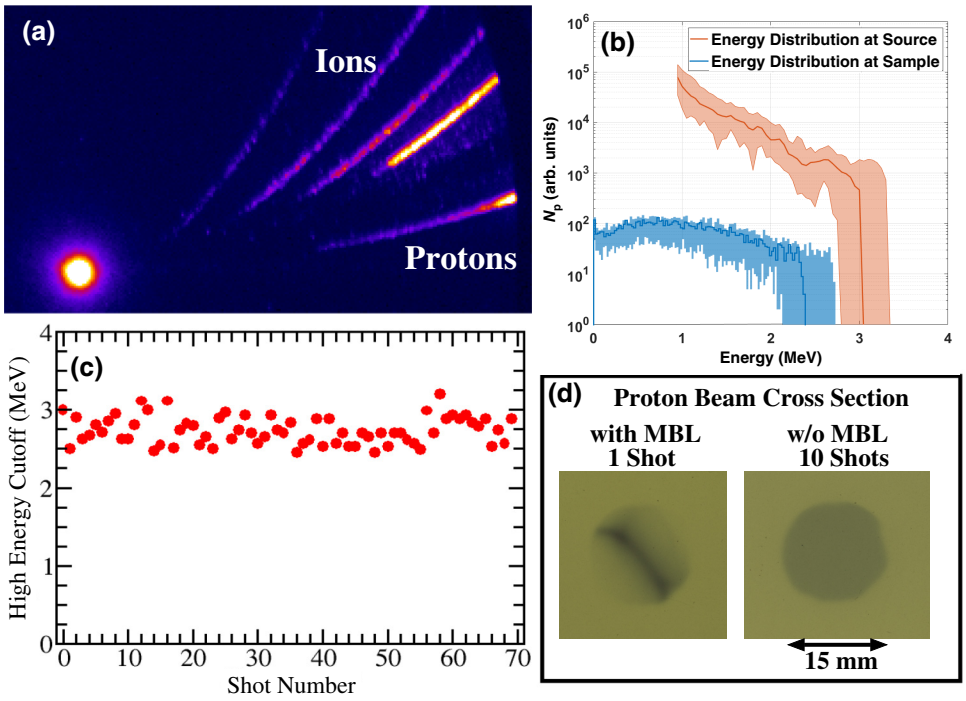

FIG. 3. Characterization of the laser-driven proton beam. (a) Typical TPS data, with the proton parabolic trace in the lower right; traces of the ions are also visible. (b) Proton-beam spectrum, as from TPS proton traces (red curve) and corresponding simulated spectra at the PIXE specimen position in air (blue curve). (c) Proton-beam high-energy cutoff estimated by TOF measurements. (d) Proton-beam cross section measured with EBT3 films with and without MBL, left and right panels, respectively.

complete damping of the laser-driven electrons is reported. In this simulation, we assumed a fast-electron beam having an exponential energy distribution, with a temperature of $T_{FE} \simeq 1.75$ MeV, i.e., the maximum value obtained by the fast-electron scaling laws theoretically and experimentally proposed in the literature (see, for instance, Ref. [53] and Refs. therein).

The energy spectrum of the proton beam from the TNSA source was characterized using a Thomson parabola spectrometer (TPS) [7,54]. For these measurements, the TPS assembly was mounted in place of the vacuum flange with the Kapton window, and its axis was set along the normal of the TNSA target (see the Supplemental Material for details [42]). Typical TPS measurement data of the laser-driven particle source under vacuum are shown in Fig. 3(a), where the proton parabolic trace is the lower one. Visible in Fig. 3(a) are also the parabolic traces of the ions that are all stopped by the Kapton window when irradiation in air is performed. In Fig. 3(b), the proton source energy spectrum, as obtained from the TPS measurements, is shown along with the corresponding simulated spectrum at the sample position, i.e., after the Kapton window and 2 cm of air. The transported proton beam in air was monitored with time-of-flight (TOF) measurements using a Si-PIN detector placed after the Kapton window along the normal of the TNSA target. The stability of the high-energy cutoff of the proton beam in air over tens of shots is shown in Fig. 3(c). It must be noted that the TPS employing a microchannel plate intensifier is more sensitive than the TOF measurement based on solid-state detectors, thereby leading to the slightly higher estimate for the cutoff energy. The two measurement sets indicate a high-energy cutoff stably around 3 MeV. During sample irradiation with an external beam, all protons from the laser-driven source with energies below 1.3 MeV were stopped in the Kapton window plus 2 cm of air, as calculated using SRIM software [55].

The total proton flux at the sample position in air was measured by means of unlaminated EBT3 radiochromic films (see the Supplemental Material for details [42]). In the left panel of Fig. 3(d) the image of the EBT3 film irradiated with a single shot using the MBL is shown. The integrated proton number over the beam cross section is estimated to be $\sim 10^7$ per shot. The observed elongated shape of the beam can be ascribed to the actual energy dependent proton beam divergence spread from the polychromatic laser-driven source [56–58]. For comparison, the image of the EBT3 irradiated with 10 shots without using the MBL is reported in the right panel of Fig. 3(d). The observed circular shape in the exposed EBT3 films is due to the aperture of the Kapton window used as vacuum-air interface. The experimentally measured enhancement flux factor with and without the MBL is about 8, in good agreement with the Monte Carlo transport simulations.

To quantitatively assess the EBL-PIXE measurements, elemental analysis of a brass (copper-zinc alloy) specimen was performed. It is noted that, to perform quantitative PIXE measurements with laser-driven protons, characteristic x-rays emitted by the laser-plasma target must be considered when performing data analysis and when choosing the TNSA target material. In fact, the characteristic x-rays emitted during high-intensity laser-matter interactions can propagate, although attenuated, up to the PIXE specimen, generating spurious PIXE-like x-ray signals via XRF. In the present case, the characteristic x-rays emitted by the Ti laser-plasma target lie in the 4.5–4.9 keV range, while the characteristic x-rays emitted by Cu and Zn in the PIXE specimens are above 8 keV, and therefore, no spurious signal is generated by XRF. In general, the characteristic x-rays emitted by the laser-plasma target and reaching the PIXE specimens must either be properly quantified and considered in the data analysis or have a lower energy than the characteristic x-rays emitted by the PIXE specimens. For example, aluminum, a typical material used as a TNSA laser-plasma target, has a characteristic x-ray emission around 1.5 keV, and therefore, can be used as a TNSA target material to perform quantitative EBL-PIXE analysis of all heavier elements.

Figure 4(a) shows the x-ray spectrum obtained by summing the signal over 39 laser shots, after correction for x-ray attenuation and for the CCD quantum efficiency (see the Supplemental Material for details [42]). We first observe that the linewidth of the x-ray line peaks is a few hundred electronvolts; this is comparable to the ones obtained for standard PIXE measurements carried out with electrostatic accelerators and silicon drift detectors [27], and it allows us to resolve the $K\alpha$ and $K\beta$ emission lines. The result of a nonlinear fit used to analyze the data points is also shown in Fig. 4(a). The fit is performed using Gaussian functions for each spectral line, with a background estimated from a quadratic fit of the data points preceding the actual x-ray lines. In most PIXE measurements, a background signal does appear, due to different processes taking place inside the PIXE sample upon proton irradiation; see Ref. [59] and Refs. therein for further details. The choice of the curve used to fit such a background around the x-ray peaks is relatively arbitrary, as studies aimed at modeling the phenomena over the entire x-ray energy range towards more precise and/or sensitive measurements are still ongoing. In our case, we choose the simplest curve, which fits our experimental background data very well in the energy range of interest. Typical for PIXE measurements, the $K\alpha$ line area was considered as a measure of the x-ray yield, Y, used for the analysis, and its ratio between Cu and Zn was found to be $Y_{\mathrm{Cu}}/Y_{\mathrm{Zn}} = 2.62$ with an estimated uncertainty of about 10%.

The ratio of the percentage atomic density from the EBL-PIXE measurement is calculated using the ratio of the x-ray yield normalized to the proton-induced K-shell

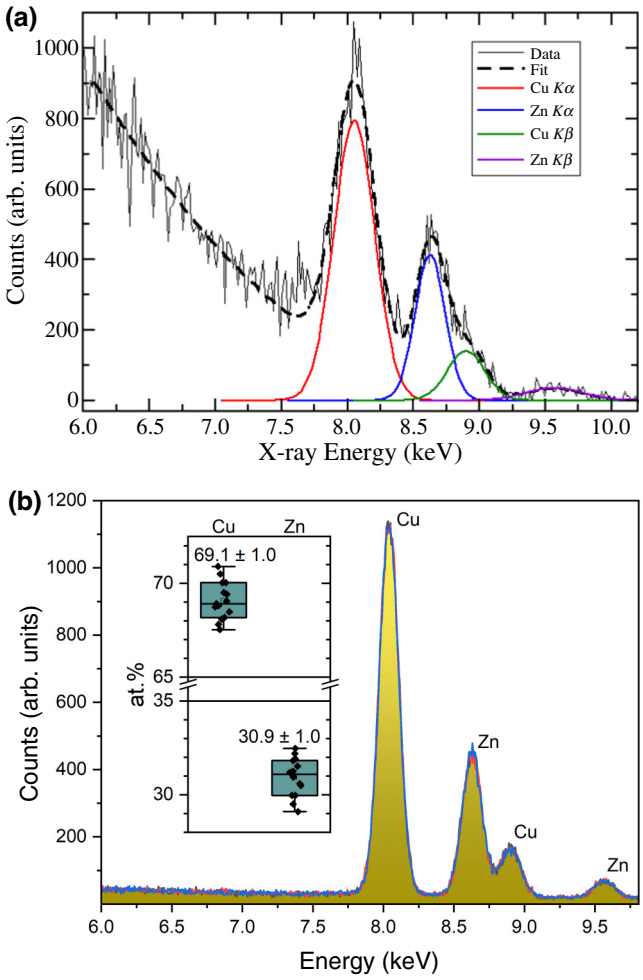

FIG. 4. (a) EBL-PIXE spectrum of the brass sample, showing the results of the fit of data points and the resulting Gaussian functions for the copper and zinc $K\alpha$ and $K\beta$ lines. (b) EDS analysis of the brass sample after 15 measurements; values reported in the inset are the average concentrations with 1% standard deviation, while boxes enclose data points from the 25% to 75% percentile, and bars indicate the full data range from maximum to minimum.

emission cross sections, σ_{Cu} and σ_{Zn}. The values for $\sigma_{\mathrm{Zn/Cu}}(E)$ in the few-MeV range are taken from Ref. [60] (see the Supplemental Material [42] for details). The actual quantitative elemental composition is then calculated by

$$\frac{N_{\mathrm{PIXE,\,Cu}}}{N_{\mathrm{PIXE,\,Zn}}} = \frac{Y_{\mathrm{Cu}}}{Y_{\mathrm{Zn}}} \times \frac{\bar{\sigma}_{\mathrm{Zn}}}{\bar{\sigma}_{\mathrm{Cu}}}, \tag{1}$$

where $\bar{\sigma}_i$ is the average cross section weighted for the proton energy spectrum, $N_p(E)$, at the sample position,

$$\bar{\sigma}_{\mathrm{Zn/Cu}} = \frac{\int N_p(E)\sigma_{\mathrm{Zn/Cu}}(E)dE}{\int N_p(E)dE}, \tag{2}$$

TABLE I. Elemental composition of the brass sample from EBL-PIXE and EDS measurements.

Technique	Copper (%)	Zinc (%)
EBL PIXE	67.8(2.5)	32.2(2.5)
EDS	69.1(1.0)	30.9(1.0)

and assuming Cu and Zn are the only constituents of the sample, as confirmed by the EDS measurement. From the spectra at the sample, as reported in Fig. 3(b), it is found that $\bar{\sigma}_{Cu}/\bar{\sigma}_{Zn} = 1.24(7)$, and the brass specimen composition obtained from EBL PIXE is $N_{PIXE,\,Cu} = 67.8\%$ and $N_{PIXE,\,Zn} = 32.2\%$ with an estimated uncertainty of 2.5%.

In Eq. (1), the effect of x-ray attenuation inside the PIXE specimens is neglected, since the energies of the characteristic x-rays emitted by Cu and Zn are quite close to each other and suffer from the same level of attenuation in the PIXE specimens. In general, however, x-ray self-absorption is an important matrix effect that must be taken into account when performing PIXE signal analysis.

EDS analysis of the brass sample through 15 measurements is reported in Fig. 4(b), resulting in average atomic density percentages of $N_{EDS,\,Cu} = 69.1\%$ and $N_{EDS,\,Zn} = 30.9\%$, with a standard deviation of 1% (see the Supplemental Material for details [42]). A comparison of the elemental composition of the brass sample measured by the EBL-PIXE and EDS techniques is summarized in Table I, showing very good agreement between the two measurements.

III. CONCLUSIONS

We have implemented and validated the external beam laser PIXE technique for nondestructive elemental analysis of specimens in air. The analysis was performed using a few tens of laser shots, and a large number ($> 10^4$) of x-ray photons per shot were acquired using a CCD detector in the single-photon regime. In our work, due to technical constraints on the laser-driven proton target system, the time needed to get the number of photons required to retrieve a PIXE spectrum spanned several minutes. As mentioned above, a laser-driven PIXE machine can be easily operated at the 10-Hz repetition rate typical of current technology, Ti:sapphire-based ultrashort 10-TW class laser systems. Over a slightly longer-term perspective, such machines may benefit from the repetition rate increasing up to the 100-Hz level, which is now technically feasible and has started to become commercially available. Although the maximum proton current of laser-driven machines remains a few orders of magnitudes smaller than that of conventional accelerators used for PIXE, it must be noted that the actual typical current used for PIXE measurements is kept well below the maximum value of the accelerator, due to issues related to both damage to the PIXE sample and the x-ray detector speed, so that typical PIXE measurements routinely performed nowadays can take minutes [61]. On the other hand, the major driver for bringing forward the case for PIXE machines based on laser-driven proton acceleration comes from considerations concerning footprint, costs, and requirements for radiation shielding. As a matter of fact, today's standard PIXE facilities are mostly based upon electrostatic accelerators, such as TANDEM machines. Although efforts are being undertaken to reduce the size and costs of these systems, they are nevertheless typically quite massive and with footprints of tens of m^2. Moreover, in such conventional systems, the whole machine is required to be hosted in a radiation-shielded area. Laser-driven proton accelerators, in contrast, although being driven by a laser system that can require an optical table of a few m^2, may relatively easily be made portable, and, importantly, allow requirements for radiation shielding to be considerably relaxed, even in view of the "accelerator stage" (focusing optics and TNSA target) being extremely compact. The present demonstration of an accurate and easy to operate nondestructive analysis methodology based on laser-driven particle accelerators will stimulate further studies and implementations of EBL PIXE towards high-sensitivity measurements, as well as support and encourage the use of laser-driven accelerators for other real practical applications.

ACKNOWLEDGMENTS

The authors acknowledge the following funding sources: Regione Toscana (POR FSE 2014-2020) and VCS srl company (Parma, Italy) with the grant "Laser-PIXE" within the research program ARCO-CNR; CNR-funded Italian research network ELI-Italy (D.M. No.631 08.08.2016); JRA ENI-CNR on Fusion Energy (CUP B34I19003070007, CNR DFM.AD006.155); EU Horizon 2020 Research and Innovation Program EuPRAXIA Preparatory Phase, under Grant Agreement No. 10107 9773; and IFAST, under Grant Agreement No. 101004730. This research has been co-funded by the European Union NextGeneration EU "Integrated Infrastructure Initiative in Photonic and Quantum Sciences", I-PHOQS (IR0000016, ID D2B8D520, and CUP B53C22001750006), and "EuPRAXIA Advanced Photon Sources", EuAPS (IR0000030 and CUP I93C21000160006).

F.B., L.L., and M.S. contributed equally to this work.

[1] H. Daido, M. Nishiuchi, and A. S. Pirozhkov, Review of laser-driven ion sources and their applications, Rep. Prog. Phys. **75**, 056401 (2012).

[2] J. Schreiber, P. R. Bolton, and K. Parodi, Hands-on laser-driven ion acceleration: A primer for laser driven source development and potential applications, Rev. Sci. Instrum. **87**, 071101 (2016).

[3] R. A. Snavely, M. H Key, S. P. Hatchett, T. E. Cowan, M. Roth, T. W. Phillips, M. A. Stoyer, E. A. Henry, T. C. Sangster, M. S. Singh, *et al.*, Intense high-energy proton beams from petawatt-laser irradiation of solids, Phys. Rev. Lett. **85**, 2945 (2000).

[4] S. C. Wilks, A. B. Langdon, T. E. Cowan, M. Roth, M. Singh, S. Hatchett, M. H. Key, D. Pennington, A. MacKinnon, and A. R. Snavely, Energetic proton generation in ultra-intense laser–solid interactions, Phys. Plasmas **8**, 542 (2001).

[5] L. A. Gizzi, D. Giove, C. Altana, F. Brandi, P. Cirrone, G. Cristoforetti, A. Fazzi, P. Ferrara, L. Fulgentini, P. Koester, *et al.*, A new line for laser-driven light ions acceleration and related TNSA studies, Appl. Sci. **7**, 984 (2017).

[6] T. Ziegler, D. Albach, C. Bernert, S. Bock, F.-E. Brack, T. E. Cowan, N. P. Dover, M. Garten, L. Gaus, R. Gebhardt, *et al.*, Proton beam quality enhancement by spectral phase control of a PW-class laser system, Sci. Rep. **11**, 7338 (2021).

[7] L. A. Gizzi, E. Boella, L. Labate, F. Baffigi, P. J. Bilbao, F. Brandi, G. Cristoforetti, A. Fazzi, L. Fulgentini, D. Giove, *et al.*, Enhanced laser-driven proton acceleration via improved fast electron heating in a controlled pre-plasma, Sci. Rep. **11**, 13728 (2021).

[8] M. Rehwald, S. Assenbaum, C. Bernert, F.-E. Brack, M. Bussmann, T. E. Cowan, C. B. Curry, F. Fiuza, M. Garten, L. Gaus, *et al.*, Ultra-short pulse laser acceleration of protons to 80 MeV from cryogenic hydrogen jets tailored to near-critical density, Nat. Commun. **14**, 4009 (2023).

[9] W. J. Ma, I. J.. Kim, J. Q. Yu, Il Woo Choi, P. K. Singh, H. W. Lee, J. H. Sung, S. K. Lee, C. Lin, Q. Liao, *et al.*, Laser acceleration of highly energetic carbon ions using a double-layer target composed of slightly underdense plasma and ultrathin foil, Phys. Rev. Lett. **122**, 014803 (2019).

[10] L. Fedeli, A. Formenti, L. Cialfi, A. Pazzaglia, and M. Passoni, Ultra-intense laser interaction with nanostructured near-critical plasmas, Sci. Rep. **8**, 3834 (2018).

[11] L. A. Gizzi, G. Cristoforetti, F. Baffigi, F. Brandi, G. D'Arrigo, A. Fazzi, L. Fulgentini, D. Giove, P. Koester, L. Labate, *et al.*, Intense proton acceleration in ultrarelativistic interaction with nanochannels, Phys. Rev. Res. **2**, 033451 (2020).

[12] G. Cristoforetti, F. Baffigi, F. Brandi, G. D'Arrigo, A. Fazzi, L. Fulgentini, D. Giove, P. Koester, L. Labate, G. Maero, *et al.*, Laser-driven proton acceleration via excitation of surface plasmon polaritons into TiO_2 nanotube array targets, Plasma Phys. Control. Fusion **62**, 114001 (2020).

[13] G. Cantono, A. Permogorov, J. Ferri, E. Smetanina, A. Dmitriev, A. Persson, T. Fülöp, and C.-G. Wahlström, Laser-driven proton acceleration from ultrathin foils with nanoholes, Sci. Rep. **11**, 5006 (2021).

[14] C. A. J. Palmer, N. P. Dover, I. Pogorelsky, M. Babzien, G. I. Dudnikova, M. Ispiriyan, M. N. Polyanskiy, J. Schreiber, P. Shkolnikov, *et al.*, Monoenergetic proton beams accelerated by a radiation pressure driven shock, Phys. Rev. Lett. **106**, 014801 (2011).

[15] A. Higginson, R. J. Gray, M. King, R. J. Dance, S. D. R. Williamson, N. M. H. Butler, R. Wilson, R. Capdessus, C. Armstrong, J. S. Green, *et al.*, Near-100 MeV protons via laser-driven transparency-enhanced hybrid acceleration scheme, Nat. Commun. **9**, 724 (2018).

[16] A. Henig, D. Kiefer, K. Markey, D. C. Gautier, K. A. Flippo, S. Letzring, R. P. Johnson, T. Shimada, L. Yin, B. J. Albright, *et al.*, Enhanced laser-driven ion acceleration in the relativistic transparency regime, Phys. Rev. Lett. **103**, 045002 (2009).

[17] R. W. Assmann, M. K. Weikum, T. Akhter, D. Alesini, A. S. Alexandrova, M. P. Anania, N. E. Andreev, I. Andriyash, M. Artioli, A. Aschikhin, *et al.*, EuPRAXIA conceptual design report, Eur. Phys. J. Spec. Top. **229**, 3675 (2020).

[18] Y. Gao, R. Liu, C.-W. Chang, S. Charyyev, J. Zhou, J. D. Bradley, T. Liu, and X. Yang, A potential revolution in cancer treatment: A topical review of FLASH radiotherapy, J. Appl. Clin. Med. Phys. **23**, e13790 (2022).

[19] L. Labate, D. Palla, D. Panetta, F. Avella, F. Baffigi, F. Brandi, F. Di Martino, L. Fulgentini, A. Giulietti, P. Köster, *et al.*, Toward an effective use of laser-driven very high energy electrons for radiotherapy: Feasibility assessment of multi-field and intensity modulation irradiation schemes, Sci. Rep. **10**, 1 (2020).

[20] L. Karsch, E. Beyreuther, W. Enghardt, M. Gotz, U. Masood, U. Schramm, K. Zeil, and J. Pawelke, Towards ion beam therapy based on laser plasma accelerators, Acta Onc. **56**, 1359 (2017).

[21] H. Schwenke, J. Knoth, P. A. Beaven, R. Kiehn, and J. Buhrz, A laser plasma x-ray source for the analysis of wafer surfaces by grazing emission x-ray fluorescence spectrometry, Spectrochim. Acta Part B **59**, 1159 (2004).

[22] F. Mirani, D. Calzolari, A. Formenti, and M. Passoni, Superintense laser-driven photon activation analysis, Commun. Phys. **4**, 185 (2021).

[23] T. M. Ostermayr, C. Kreuzer, F. S. Englbrecht, J. Gebhard, J. Hartmann, A. Huebl, D. Haffa, P. Hilz, K. Parodi, and J. Wenz, *et al.*, Laser-driven x-ray and proton micro-source and application to simultaneous single-shot bi-modal radiographic imaging, Nat. Commun. **11**, 6174 (2020).

[24] T. L. Audet, A. Alejo, L. Calvin, M. H. Cunningham, G. R. Frazer, G. Nersisyan, M. Phipps, J. R. Warwick, G. Sarri, and N. A. M. Hafz, *et al.*, Ultrashort, MeV-scale laser-plasma positron source for positron annihilation lifetime spectroscopy, Phys. Rev. Accel. Beams **24**, 073402 (2021).

[25] S. A. E. Johansson, J. L. Campbell, and K. G. Malmqvist, eds., *Particle-Induced X-Ray Emission Spectrometry (PIXE)* (Wiley, New York, 1995).

[26] H. R. Verma, *Atomic and Nuclear Analytical Methods XRF, Mössbauer, XPS, NAA and Ion-Beam Spectroscopic Techniques* (Springer-Verlag, Berlin Heidelberg, 2007).

[27] M. R. J. Palosaari, M. Käyhkö, K. M. Kinnunen, M. Laitinen, J. Julin, J. Malm, T. Sajavaara, W. B. Doriese, J. Fowler, C. Reintsema, *et al.*, Broadband ultrahigh-resolution spectroscopy of particle-induced x rays: Extending the limits of nondestructive analysis, Phys. Rev. Appl. **6**, 024002 (2016).

[28] F. Lucarelli, G. Calzolai, M. Chiari, M. Giannoni, D. Mochi, S. Nava, and L. Carraresi, The upgraded external-beam PIXE/PIGE set-up at LABEC for very fast measurements on aerosol samples, Nucl. Instrum. Methods Phys. Res. B **318**, 55 (2014).

[29] F. Lucarelli, G. Calzolai, M. Chiari, S. Nava, and L. Carraresi, Study of atmospheric aerosols by IBA techniques: The LABEC experience, Nucl. Instrum. Methods Phys. Res. B **417**, 121 (2018).
[30] T. Sakai, M. Oikawa, T. Sato, T. Nagamine, H. D. Moon, K. Nakazato, and K. Suzuki, New in-air micro-PIXE system for biological applications, Nucl. Instrum. Methods Phys. Res. B **231**, 112 (2005).
[31] M. Chiari, External beam IBA measurements for cultural heritage, Appl. Sci. **13**, 3366 (2023).
[32] F. Taccetti, L. Castelli, M. Chiari, C. Czelusniak, S. Falciano, M. Fedi, F. Giambi, P. A. Mandò, M. Manetti, M. Massi, *et al.*, MACHINA, the movable accelerator for cultural heritage *in-situ* non-destructive analysis: Project overview, Rend. Lincei Sci. Fis. **34**, 427 (2023).
[33] A. Maffini, F. Mirani, M Galbiati, K. Ambrogioni, F. Gatti, M. S. G. De Magistris, D. Vavassori, D. Orecchia, D. Dellasega, V. Russo, *et al.*, Towards compact laser-driven accelerators: Exploring the potential of advanced double-layer targets, EPJ Tech. Instrum. **10**, 15 (2023).
[34] F. Mirani, A. Maffini, and M. Passoni, Laser-driven neutron generation with near-critical targets and application to materials characterization, Phys. Rev. Appl. **19**, 044020 (2023).
[35] M. Barberio and P. Antici, Laser-PIXE using laser-accelerated proton beams, Sci. Rep. **9**, 6855 (2019).
[36] M. Passoni, F. M. Arioli, L. Cialfi, D. Dellasega, L. Fedeli, A. Formenti, A. C. Giovannelli, A. Maffini, F. Mirani, A. Pazzaglia, *et al.*, Advanced laser-driven ion sources and their applications in materials and nuclear science, Plasma Phys. Control. Fusion **62**, 014022 (2020).
[37] M. Passoni, L. Fedeli, and F. Mirani, Superintense laser-driven ion beam analysis, Sci. Rep. **9**, 9202 (2019).
[38] F. Boivin, S. Vallières, S. Fourmaux, S. Payeur, and P. Antici, Quantitative laser-based x-ray fluorescence and particle-induced x-ray emission, New J. Phys. **24**, 053018 (2022).
[39] P. Puyuelo-Valdes, S. Vallières, M. Salvadori, S. Fourmaux, S. Payeur, J.-C. Kieffer, F. Hannachi, and P. Antici, Combined laser-based x-ray fluorescence and particle-induced x-ray emission for versatile multi-element analysis, Sci. Rep. **11**, 9998 (2021).
[40] F. Mirani, A. Maffini, F. Casamichiela, A. Pazzaglia, A. Formenti, D. Dellasega, V. Russo, D. Vavassori, D. Bortot, M. Huault, *et al.*, Integrated quantitative PIXE analysis and EDX spectroscopy using a laser-driven particle source, Sci. Adv. **7**, eabc8660 (2021).
[41] L. A. Gizzi, L. Labate, F. Baffigi, F. Brandi, G. Bussolino, L. Fulgentini, P. Koester, and D. Palla, Overview and specifications of laser and target areas at the Intense Laser Irradiation Laboratory, High Power Laser Sci. Eng. **9**, E10 (2021).
[42] See the Supplemental Material http://link.aps.org/supplemental/10.1103/PhysRevApplied.21.064020 for technical details on the experimental apparatus and procedures, determination of the x-ray transmission factor, and the x-ray emission cross section; it also includes Refs. [62–66].
[43] J. Bin, L. Obst-Huebl, J.-H. Mao, K. Nakamura, L. D. Geulig, H. Chang, Q. Ji, L. He, J. De Chant, Z. Kober, *et al.*, A new platform for ultra-high dose rate radiobiological research using the BELLA PW laser proton beamline, Sci. Rep. **12**, 1484 (2022).
[44] N. Xu, M. J. V. Streeter, O. C. Ettlinger, H. Ahmed, S. Astbury, M. Borghesi, N. Bourgeois, C. B. Curry, S. J. D. Dann, N. P. Dover, *et al.*, Versatile tape-drive target for high-repetition-rate laser-driven proton acceleration, High Power Laser Sci. Eng. **11**, e23 (2023).
[45] A. Groza, A. Chirosca, E. Stancu, B. Butoi, M. Serbanescu, D. B. Dreghici, and M. Ganciu, Assessment of angular spectral distributions of laser accelerated particles for simulation of radiation dose map in target normal sheath acceleration regime of high power laser-thin solid target interaction–comparison with experiments, Appl. Sci. **10**, 4390 (2020).
[46] A. Mancic, J. Robiche, P. Antici, P. Audebert, C. Blancard, P. Combis, F. Dorchies, G. Faussurier, S. Fourmaux, M. Harmand, *et al.*, Isochoric heating of solids by laser-accelerated protons: Experimental characterization and self-consistent hydrodynamic modeling, High Energy Density Phys. **6**, 21 (2010).
[47] M. Nishiuchi, I. Daito, M. Ikegami, H. Daido, M. Mori, S. Orimo, K. Ogura, A. Sagisaka, A. Yogo, A. S. Pirozhkov, *et al.*, Focusing and spectral enhancement of a repetition-rated, laser-driven, divergent multi-MeV proton beam using permanent quadrupole magnets, Appl. Phys. Lett. **94**, 061107 (2009).
[48] G. A. P. Cirrone, G. Cuttone, F. Romano, F. Schillaci, V. Scuderi, A. Amato, G. Candiano, M. Costa, G. Gallo, G. Larosa, *et al.*, Design and status of the ELIMED beam line for laser-driven ion beams, Appl. Sci. **5**, 427 (2015).
[49] L. Labate, A. Giulietti, D. Giulietti, P. Köster, T. Levato, L. A. Gizzi, F. Zamponi, A. Lübcke, T. Kämpfer, *et al.*, Novel x-ray multispectral imaging of ultraintense laser plasmas by a single-photon charge coupled device based pinhole camera, Rev. Sci. Instrum. **78**, 103506 (2007).
[50] L. Labate, M. Galimberti, A. Giulietti, D. Giulietti, L. A. Gizzi, P. Tomassini, and G. Di Cocco, A laser-plasma source for CCD calibration in the soft x-ray range, Nucl. Instrum. Methods Phys. Res. A **495**, 148 (2002).
[51] J. Allison, K. Amako, J. Apostolakis, P. Arce, M. Asai, T. Aso, E. Bagli, A. Bagulya, S. Banerjee, G. Barrand, *et al.*, Recent developments in Geant4, Nucl. Instrum. Methods Phys. Res. A **835**, 186 (2016).
[52] F. Brandi, L. Labate, D. Palla, S. Kumar, L. Fulgentini, P. Koester, F. Baffigi, M. Chiari, D. Panetta, and L. A. Gizzi, A few MeV laser-plasma accelerated proton beam in air collimated using compact permanent quadrupole magnets, Appl. Sci. **11**, 6358 (2021).
[53] M. G. Haines, M. S. Wei, F. N. Beg, and R. B. Stephens, Hot-electron temperature and laser-light absorption in fast ignition, Phys. Rev. Lett. **102**, 045008 (2009).
[54] L. A. Gizzi, F. Baffigi, F. Brandi, G. Bussolino, G. Cristoforetti, A. Fazzi, L. Fulgentini, D. Giove, P. Koester, L. Labate, *et al.*, Light ion accelerating line (L3IA): Test experiment at ILIL-PW, Nucl. Instrum. Methods Phys. Res. A **909**, 160 (2018).
[55] F. J. Ziegler, M. D. Ziegler, and J. P. Biersack, SRIM – the stopping and range of ions in matter (2010), Nucl. Instrum. Methods Phys. Res. B **268**, 1818 (2010).

[56] F. Schillaci, L. Pommarel, F. Romano, G. Cuttone, M. Costa, D. Giove, M. Maggiore, A. D. Russo, V. Scuderi, V. Malka, *et al.*, Characterization of the ELIMED permanent magnets quadrupole system prototype with laser-driven proton beams, J. Instrum. **11**, T07005 (2016).

[57] H. Sakaki, M. Nishiuchi, T. Hori, P. R. Bolton, A. Yogo, M. Katagiri, K. Ogura, A. Sagisaka, A. S. Pirozhkov, S. Orimo, *et al.*, Prompt in-line diagnosis of single bunch transverse profiles and energy spectra for laser-accelerated ions, Appl. Phys. Express **3**, 126401 (2010).

[58] M. Wu, J. Zhu, D. Li, T. Yang, Q. Liao, Y. Geng, X. Xu, C. Li, Y. Shou, Y. Zhao, *et al.*, Collection and focusing of laser accelerated proton beam by an electromagnetic quadrupole triplet lens, Nucl. Instrum. Methods Phys. Res. A **955**, 163249 (2020).

[59] K. Murozono, K. Ishii, H. Yamazaki, S. Matsuyama, and S. Iwasaki, PIXE spectrum analysis taking into account bremsstrahlung spectra, Nucl. Instrum. Methods Phys. Res. B **150**, 76 (1999).

[60] H. Paul and J. Sacher, Fitted empirical reference cross sections for K-shell ionization by protons, At. Data Nucl. Data Tables **42**, 105 (1989).

[61] S. Aljboor, A. Angyal, D. Baranyai, E. Papp, M. Szarka, Z. Szikszai, I. Rajta, I. Vajda, and Z. Kertesz, Light-element sensitive in-air millibeam PIXE setup for fast measurement of atmospheric aerosol samples, J. Anal. At. Spectrom. **38**, 57 (2023).

[62] M. Schollmeier, M. Geissel, A. B. Sekfow, and K. A. Filippo, Improved spectral data unfolding for radiochromic film imaging spectroscopy of laser-accelerated proton beams, Rev. Sci. Instrum. **85**, 043305 (2014).

[63] S. Devic, N. Tomic, and D. Lewis, Reference radiochromic film dosimetry: Review of technical aspects, Phys. Med. **32**, 541 (2016).

[64] S. Devic and D. J. Brenner, LET dependent response of GafChromic films investigated with MeV ion beams, Phys. Med. Biol. **63**, 245021 (2018).

[65] Md. R. Khan, D. Crumpton, and P. E. Francois, Proton-induced x-ray production in titanium, nickel, copper, molybdenum and silver, J. Phys. **B9**, 455 (1976).

[66] Md. R. Khan, A. G. Hopkins, D. Crumpton, and P. E. Francois, Proton-induced x-ray production in vanadium, iron, zinc, gallium, yttrium, cadmium, indium and tin, X-Ray Spect. **6**, 140 (1977).